

1                   MTSCCleav: a Multivariate Time Series  
2                   Classification (MTSC)-based method for  
3                   predicting human Dicer cleavage sites

4                   First Author<sup>1,2\*</sup>, Second Author<sup>2,3†</sup> and Third Author<sup>1,2†</sup>

5                   <sup>1</sup>\*Department, Organization, Street, City, 100190, State, Country.

6                   <sup>2</sup>Department, Organization, Street, City, 10587, State, Country.

7                   <sup>3</sup>Department, Organization, Street, City, 610101, State, Country.

8                   \*Corresponding author(s). E-mail(s): [iauthor@gmail.com](mailto:iauthor@gmail.com);  
9                   Contributing authors: [iiauthor@gmail.com](mailto:iiauthor@gmail.com); [iiiauthor@gmail.com](mailto:iiiauthor@gmail.com);

10                  †These authors contributed equally to this work.

11                  **Abstract**

12                  **Background:** MicroRNAs (miRNAs) are small non-coding RNAs (ncRNAs)  
13                  that regulate gene expression at the post-transcriptional level, thereby playing  
14                  essential roles in diverse biological processes. The biogenesis of miRNAs requires  
15                  dicer to cleave at specific sites on the precursor miRNAs (pre-miRNAs). Several  
16                  machine learning approaches have been proposed to predict whether an input  
17                  sequence contains a cleavage site. However, they rely heavily on complex feature  
18                  engineering or opaque deep neural networks. It results in a lack of generalizability  
19                  and a long running time. There is a need for an alternative modeling paradigm  
20                  that is accurate, fast, and simple.

21                  **Results:** We proposed a novel approach to frame the task as a multivariate time  
22                  series classification problem. Various encoding methods have been proposed to  
23                  convert the sequence and the predicted secondary structure into a time series.  
24                  We also leveraged the probabilities of the base pairs in the predicted secondary  
25                  structure. Computational experiments demonstrate that our proposed method  
26                  can achieve better or comparable results using a simpler, more intuitive model  
27                  and less computational time. It achieves 3.7X ~ 28.8X speedup. Through per-  
28                  turbation experiments, we found that regions close to the center of pre-miRNAs  
29                  are essential for predicting human dicer cleavage sites.

30                  **Conclusion:** By transforming the RNA sequence and its secondary structure  
31                  information into a time series and utilizing simple, state-of-the-art time series  
32                  classifiers, we achieved comparable or even superior performance in a simpler

33 and faster manner. Code is available at: <https://github.com/cyuab/time-series-classification-cleavage>.  
34

35 **Keywords:** miRNA, Dicer Cleavage Site, Genomic signal processing (GSP),  
36 (Multivariate) time Series Classification (MTSC, TSC)

## 37 1 Background

38 One of the most important theories in molecular biology is the central dogma. It  
39 depicts the flow of genetic information [1, 2]. Proteins are the functional units. And  
40 the information stored in DNA is used to create them. Genes (segments) in DNA are  
41 used as templates for messenger RNAs (mRNAs) synthesis. An mRNA acts as a set  
42 of instructions to assemble a chain of amino acids, which form a linear polypeptide.  
43 To become biologically active, this chain is folded into a specific 3D structure, a  
44 proper configuration that enables it to perform its desired functions. And this folded  
45 polypeptide is called a functional protein, or simply a protein. This entire process  
46 closely resembles how a computer program runs on a machine. The source code does  
47 not function by itself. First, it is translated into assembly code (a lower-level, less  
48 human-readable form) and then into an executable file that can actually perform the  
49 intended tasks [3].

50 These mRNAs are called “coding RNAs” because they code for proteins. There are  
51 other genes in which the final product is the RNA molecule itself. They are called non-  
52 coding RNAs (ncRNAs). Two types of small ncRNAs are particularly important. They  
53 are microRNAs (miRNAs) and small interfering RNAs (siRNAs). Their discovery was  
54 recognized with the 2006 Nobel Prize in Physiology or Medicine<sup>1</sup>, awarded for work  
55 completed only eight years prior [1].

56 In this study, we focus on miRNAs. A miRNA can regulate the expression of  
57 several proteins. Hence, understanding the biogenesis of miRNAs is of great value. It  
58 involves the processing of primary miRNAs (pri-miRNAs). RNAs are 3D molecules.  
59 We can understand their properties by analyzing their 1D sequence or 2D structure,  
60 known as secondary structure. RNA sequence is easily obtained through sequencing.  
61 The sequence and its predicted secondary structure of a pri-miRNA “hsa-let-7a-1” is  
62 shown in Fig. 1.

63 Recall that a pri-miRNA contains a hairpin loop, also called a stem loop. A  
64 microprocessor complex comprising Drosa and DCR8 cleaves the pri-miRNA to  
65 form a precursor miRNA (pre-miRNA) inside the nucleus. The stem-loop is still pre-  
66 served, but the two arms become shorter. After that, the pri-miRNA is transported  
67 by Exportin 5 from the nucleus to the cytoplasm. It is further cleaved by an enzyme  
68 called dicer [4]. Dicer cleaves the stem-loop from the two arms at the two cleavage  
69 sites, shown as the two scissors in Fig. 1. The stem-loop is removed. It results in a short

---

<sup>1</sup>The Nobel Prize in Physiology or Medicine 2006 - NobelPrize.org:

<https://www.nobelprize.org/prizes/medicine/2006/summary/> (Accessed on: 2025-06-13).

<sup>2</sup>Its miRBase entry: <https://mirbase.org/hairpin/MI0000060>. (Accessed on: 2025-06-12).

<sup>3</sup>RNAfold web server: <http://rna.tbi.univie.ac.at/cgi-bin/RNAWebSuite/RFNAfold.cgi>. (Accessed on: 2025-06-12). The figure is viewed in “forna”. This view option can be chosen on the website.

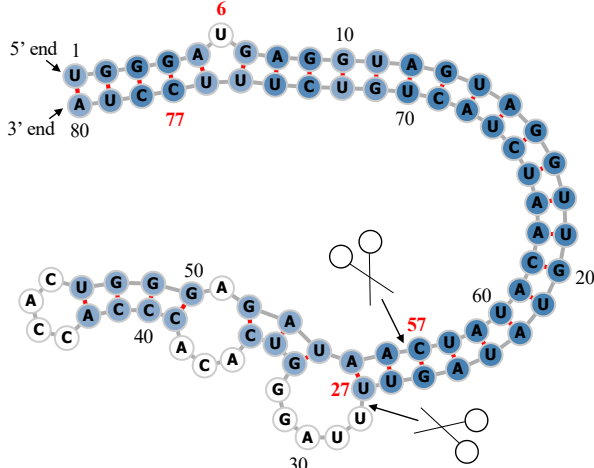


**Fig. 1:** Predicted secondary structure of the sequence  $S$  of pri-miRNA “hsa-let-7a-1”<sup>2</sup>. Experimental evidence suggests that the two deviated mature miRNAs are  $UGA \cdots GUU$  and  $CUA \cdots UUC$ . They are  $S(6 : 27)$  and  $S(57 : 77)$  (Both ends are inclusive.). The ends are highlighted in **bold**. Since  $S(6 : 27)$  ( $S(57 : 77)$ ) is near the 5' (3') end, we call it “5p (3p) mature miRNA”. The two scissors indicate the two cleavage sites. The color intensity of the nodes reflects their base pair probability in this predicted secondary structure. The deeper the color, the higher the probability. The unpaired nodes are uncolored. The raw figure is generated by RNAfold web server<sup>3</sup>.

70 double-stranded miRNA molecule, known as a miRNA duplex, which consists of the  
 71 5p strand and the 3p strand<sup>4</sup>. These molecules may be subjected to additional trim-  
 72 ming. The miRNA duplex is loaded into an RNA-induced silencing complex (RISC).  
 73 RISC unwinds the duplex and tends to retain the strand with the less stable 5' end as  
 74 the guide strand. The other strand is called the passenger strand. The retained strand  
 75 guides the RISC to silence the target mRNA. Note that both strands can become the  
 76 guide strand.

77 Dicer plays an important role in the biogenesis of miRNAs. It is reasonable to  
 78 argue that the structure of the pre-miRNAs informs dicer about the cleavage pro-  
 79 cess. It would be of great benefit to understand how dicer selects cleavage sites from  
 80 the neighborhood information near the cleavage sites. Studies [5–7] revealed that the  
 81 secondary structures are essential for cleavage site determination. Hence, to predict  
 82 or classify whether a subsequence, extracted from the sequence of a pri-miRNA,  
 83 contains a cleavage site, we can make use of both the sequence and secondary structure  
 84 information. PHDcleav employed support vector machines (SVM), leveraging sequence  
 85 and structure-based features [8] for the classification. LBSizeCleav improved upon  
 86 it by considering the loop and bulge lengths [9]. [10] proposed an ensemble learn-  
 87 ing approach, using a gradient boosting machine for better accuracy. [11] developed  
 88 a deep learning model, namely DiCleave. This model used an autoencoder to learn

<sup>4</sup>The 5p strand comes from the 5' arm while the 3p strand comes from the 3' arm. For the directionality, the 5p (3p) strand retains the original 5' (3') end of the pre-miRNA.

89 the secondary structure embeddings of pre-miRNAs from all the species in the miR-  
90 Base database and leveraged this information. All these methods begin with curated  
91 pre-miRNA sequences from the miRBase database. Their secondary structures are pre-  
92 dicted. Patterns are extracted from the sequence and the secondary structure. They  
93 create the positive cleavage patterns by setting the cleavage sites at the middle of the  
94 patterns. The follow-up work of [11], which created the cleavage pattern by allow-  
95 ing cleavage sites to appear at any position within the pattern, instead of the middle  
96 only [12]. It created a much larger dataset. This increased dataset facilitates the learn-  
97 ing of the deep learning method at the cost of increased running time. We utilized  
98 the original dataset setting [8–11]. DiCleave is the current state-of-the-art (SOTA) for  
99 this problem with the original dataset setting.

100 These models suffer several limitations. They rely heavily on complicated feature  
101 engineering or opaque deep learning models [10–12]. It results in a lack of generaliz-  
102 ability and a long running time. There is a need to design a simpler model so that it  
103 can be easily extended to other prediction tasks on RNA data. One way to analyze  
104 sequence data is to transform it into time series data. In response to this, we proposed  
105 a multivariate time series classification-based method. Our contributions are shown as  
106 follows.

- 107 1. To the best of our knowledge, we are the first to frame the prediction of the cleavage  
108 sites as a multivariate time series classification problem.
- 109 2. We introduced several encoding methods to convert RNA data to time series.
- 110 3. We proposed utilizing the base-pair probabilities in the predicted secondary struc-  
111 ture for the prediction. To our surprise, this information has been ignored in the  
112 existing works.
- 113 4. We conducted perturbation-based experiments. It shows that regions close to the  
114 cleavage sites are important for this problem. It agrees with the existing study [10].

## 115 2 Methods

116 The overall pipeline of this study is summarized in Fig. 2.

### 117 2.1 Data Preparation

118 We used miRBase database [13]<sup>5</sup>. The database comprises miRNA data from various  
119 organisms [14]. The database contains 38589 miRNA records. Each record refers to  
120 a miRNA sequence, along with other properties such as name, accession, organism,  
121 and information on its derivative miRNA products. We are interested in pri-miRNA  
122 in humans. The derivative miRNA products are the mature miRNAs. The database  
123 also annotates the location of the mature miRNA within the original sequence and  
124 indicates whether its existence has experimental evidence.

125 Table 1 shows its four representative records. We first selected the records from  
126 humans (*Homo sapiens*). It resulted in 1917 records. To identify the actual locations

---

<sup>5</sup>The website is [www.mirbase.org](http://www.mirbase.org), and the newest version of the database is Release 22.1 (Accessed on 2025-06-22).

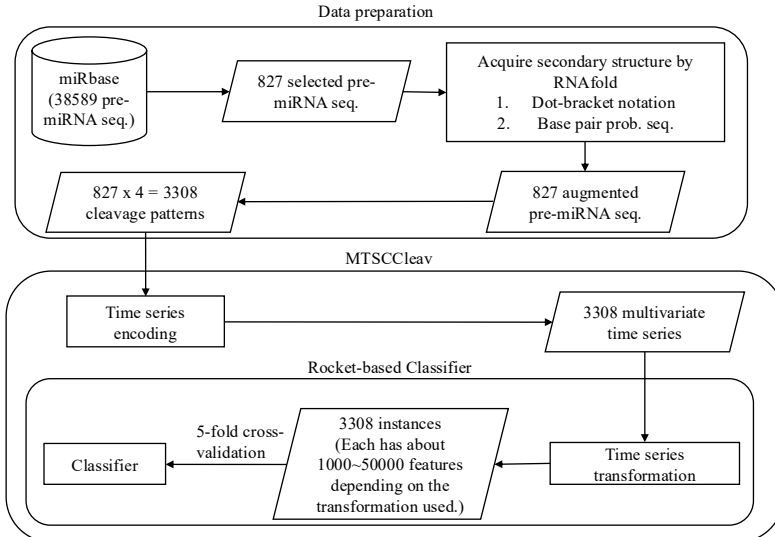


**Fig. 2:** The overall pipeline of this study. Symbol notations: Cylinder - Dataset, Rectangle - Process, Parallelogram - Input / Output, Rounded Rectangle - Component.

Accession	Name	Organism	Sequence	Mature miRNA 1	Mature miRNA 2
MI0000001	cel-let-7	Caenorhabditis elegans	<i>UACAC...UUCGA</i>	cel-let-7-5p 17:38 experimental	cel-let-7-3p 60:81 experimental
<b>MI0000060</b>	hsa-let-7a-1	Homo sapiens	<i>UGGGA...UCCUA</i>	hsa-let-7a-5p 6:27 experimental	hsa-let-7a-3p 57:77 experimental
MI0000114	hsa-mir-107	Homo sapiens	<i>CUCUC...ACAGA</i>	hsa-miR-107 50:72 experimental	NA
MI0000238	hsa-mir-196a-1	Homo sapiens	<i>GUGAA...UUCAC</i>	hsa-miR-196a-5p 7:28 experimental	hsa-miR-196a-1-3p 45:65 not experimental

**Table 1:** Selected representative records from miRBase. For the last two columns, the first line shows the name, the second line shows its location in the original sequence, and the third line indicates whether its existence has experimental evidence. The selected one is highlighted in **bold**.

of the two cleavage sites in the pri-miRNA sequence supported by experimental evidence, we selected records that have two mature miRNAs resulting from cleavage at the 5p arm and the 3p arm, both of which have experimental support. Hence, only “MI0000060” (“hsa-let-7a-1”) would be selected in the table. It would serve as our running example. The whole sequence of it is listed in Table 2. After the selection process, we selected 827 experimental validated pre-miRNA sequences, each with its two mature miRNA products. This formed our dataset.

Sequence	Secondary Structure (In Dot-bracket notation)
1 UGGGA <b>UGAGGUAGUAGGUUGUAUAGUU</b> 27 28 UUAGGGUCACACCCACCACUGGGAGAU 54 55 AAC <b>CUAUACAAUCUACUGCUUUUC</b> CUA 80	1 (((((.((((((((((((( 27 28 UUAGGGUCACACCCACCACUGGGAGAU 54 55 ))))))))))))))))))))) 80
Base-pair probabilities sequence (the first 10 bases)	
1 (0.549, 0.946, 0.987, 0.987, 0.904) 5 6 ( <b>0.000</b> , 0.841, 0.974, 0.981, 0.890) 10	

**Table 2:** The whole sequence of “hsa-let-7a-1” and its predicted secondary structure by RNAfold. The corresponding positions of the two mature miRNAs and the probability of the unpaired “U” are highlighted in **bold**.

### 134 2.1.1 Argument the dataset with Secondary Structure information

135 We leveraged the predicted secondary structure of these sequences to enhance the  
 136 accuracy of the classification. Recall that a specific three-dimensional (3D) structure  
 137 is required for DNA, RNA, and protein to perform functions [15]. However, finding  
 138 these 3D structures using experimental methods is costly and time-consuming. Hence,  
 139 prediction methods for such 3D structures are necessary and helpful for downstream  
 140 analysis. However, predicting the 3D structures is challenging. One of the reasons  
 141 is that there are some “nonconventional” base-pair interactions that allow an RNA  
 142 sequence to fold into a 3D structure. The local structures of the 3D structures, the  
 143 secondary structures, only focus on the conventional base-pair interactions [2]. Hence,  
 144 predicting secondary structures is easier and faster. We employed RNAfold from the  
 145 ViennaRNA Package<sup>6</sup> to predict the secondary structure for a given pri-miRNA  $S$  [16].  
 146 RNAfold returns the secondary structure in the dot-bracket notation and a matrix  
 147 of base-pair probabilities. The matrix is a square matrix with the side length  $|S|$ ,  
 148 where each entry  $m_{ij}$  is the probability of base  $s_i$  paired up with base  $s_j$ . Dot-bracket  
 149 notation is a way of representing the secondary structure of  $S$ . Open parentheses “(”  
 150 (Close parentheses “)”)) indicates that the base is paired with a complementary base  
 151 further (earlier) along in  $S$ . Dot “.” indicates that the base is unpaired. Equipped with  
 152 the matrix, we can construct the base-pair probability sequence of  $S$ . The predicted  
 153 secondary structure and the base-pair probability sequence of our running example  
 154 are shown in Table 2.

### 155 2.1.2 Extract cleavage patterns

156 The locations of the two mature miRNAs on the whole sequence indicate the probable  
 157 locations of the two cleavage sites. The 5p cleavage site must be beyond and near the  
 158 ending location of the 5p mature miRNA. We deemed the immediate bond next to  
 159 the 5p mature miRNA’s ending position the 5p cleavage site, with the knowledge that  
 160 the actual cleavage site may not be this immediate bond but rather the nearby bonds  
 161 after it. The same applies to the 3p cleavage site. It is located at the immediate bond  
 162 before the starting position of the 3p mature miRNA.

<sup>6</sup>The latest stable release is Version 2.7.0 (Accessed on 2025-06-22).

163 For each arm of each whole sequence, we extracted a 14-string<sup>7</sup> with the cleavage  
 164 site located at the center of the string. The first 7 nt (nucleotide) before the center are  
 165 highlighted in **bold**. In our running example, it would be “**UAUAGUU**UUAGGU”  
 166 for the 5p cleavage site and “**GAGAUAA**CUAUACA” for the 3p cleavage site.  
 167 We refer to these 14-strings as cleavage patterns. We also generate non-cleavage  
 168 patterns by selecting a 14-string with the center 6 nt away from the corresponding  
 169 cleavage sites towards the corresponding mature miRNA [9, 10] for each arm  
 170 of each whole sequence. So, in our running example, the 5p non-cleavage pat-  
 171 tern would be “**AGGUUGU**AUAGUUU”. The 3p non-cleavage pattern would be  
 172 “**ACUAUAC**AAUCUAC”.

173 In conclusion, for a given pri-miRNA sequence, we can generate two cleavage pat-  
 174 terns and two non-cleavage patterns. We call these four patterns simply the “four  
 175 strings” of a given pri-miRNA. We also call each string a strand. The “four strings”  
 of our running example are listed in Table 3.

	5p cleav	5p non-cleav	3p cleav	3p non-cleav
Input strand	<b>UAUAGUU</b> UUAGGU	<b>AGGUUGU</b> AUAGUUU	<b>GAGAUAA</b> CUAUACA	<b>ACUAUAC</b> AAUCUAC
Complementary strand	AUAUCAA_____UA	UCUAACAUAAUCAA_	C_CUGUUGAU AUGU	UGAUUAUGUUGGAUG

**Table 3:** The first row shows the “four strings” of “hsa-let-7a-1”. Their complementary strands are shown in the second row. As a whole, they are referred to as the “eight strings”.

176  
 177 We can construct the complementary strand of each of the strands in the “four  
 178 strings” by finding the corresponding paired base for each of the bases in the input  
 179 strand by considering the secondary structure information. We use “\_” to denote the  
 180 unpaired base in the complementary strand. For example, in Fig. 1, “UUAGG” in the  
 181 5p cleavage pattern is unpaired, while other bases pair with some bases, the resulting  
 182 complementary strand is “AUAUCAA\_\_\_\_\_UA”. There is a loop/ budge there. We  
 183 refer to the “four strings” and the four complementary strands together as the “eight  
 184 strings” of the input pre-miRNA. It is also shown in Table 3.

## 185 2.2 Time Series Encoding

186 A time series  $T = t_1, t_2, \dots, t_n$  is a sequence of real-valued numbers<sup>8</sup>. A short contiguous  
 187 region of  $T$  is called a subsequence. A subsequence  $T(i:j) = t_i, t_{i+1}, \dots, t_j$  of a time  
 188 series  $T$  is a shorter time series that starts from position  $i$  and ends at position  $j$ ,  
 189 where  $i < j$ .

190 Strings and time series are temporal sequences. The difference between strings and  
 191 time series lies in their behavioral attributes [17]. For strings, an entry is a letter from  
 192 a predefined set called the alphabet. For example, the alphabet is  $\{A, C, G, T\}$  in the  
 193 DNA string, while  $\{A, C, G, U\}$  in the RNA string. For time series, an entry is a real

<sup>7</sup>String with length = 14.

<sup>8</sup>We use the small letter (e.g.,  $t$ ) of the variable name of time series (e.g.,  $T$ ) for the entries.

number. Unlike real numbers, there is no ordering in the alphabet unless some external domain knowledge is introduced.

The study of applying signal processing techniques to genomic data is called “Genomic Signal Processing” (GSP) [18, 19]. In the field of GSP, the time series representations of DNA strings are referred to as DNA numeric representations (DNR). Many DNRs have been proposed. We noted that DNA strings and RNA strings are equivalent from a computational standpoint. Many transformation methods designed for DNA can be applied to RNA by simply substituting  $T$  with  $U$ . We present nine encoding methods. The relationship among them is shown in Fig. 3.

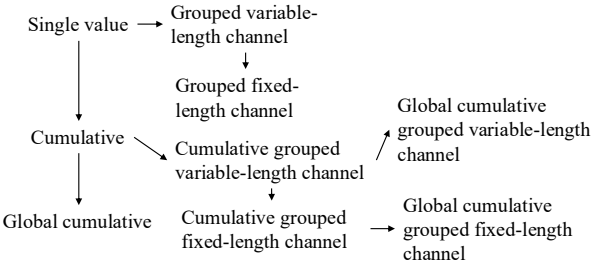


**Fig. 3:** Relationship of the proposed encoding methods.

202

### 203 2.2.1 Single value versus Cumulative

204 One of the simple, if not the simplest, encoding is to map the letters into numbers  
 205 without considering any domain knowledge. This approach is called the “Single value  
 206 mapping” [18, 20–23]. One single value is assigned to each of the letters. Domain  
 207 knowledge can be utilized. [24] employed the atomic number of each nucleotide as the  
 208 transformed values, where  $\{G = 78, A = 70, C = 58, T = 66\}$ . [25] used electron-ion  
 209 interaction potential representation (EIIP) as such value, where  $\{G = 0.0806, A =$   
 210  $0.1260, C = 0.1340, T = 0.1335\}$ . Our goal is to transform the input strand and its  
 211 complementary strand into time series, aiming to capture the information contained  
 212 in these sequences and the secondary structure implied by them. We employed the  
 213 following reasoning to assign the value:

- 214 1. We employ the complementary property [22, 26] during encoding. Recall that in  
 215 the base-pairing rules,  $G$  pairs with  $C$  to form three hydrogen bonds while  $A$  pairs  
 216 with  $U$ <sup>9</sup> to form two hydrogen bonds.  $G-C$  pairs are more stable than  $A-U$  pairs.  $G$   
 217 ( $U$ ) can be regarded as the “inverse” of  $C$  ( $A$ ). We can preserve these base-pairing  
 218 rules in the encoding by assigning  $G$  ( $A$ ) and  $C$  ( $U$ ) opposite values.
- 219 2.  $G$  and  $A$  have a two-ring structure. They are purines.  $C$  and  $U$  have a single-ring  
 220 structure. They are pyrimidines. Hence, we put  $G$  and  $A$  ( $C$  and  $U$ ) on the same  
 221 side of the number line with zero in the middle.

---

<sup>9</sup>In DNA,  $A$  pairs with  $T$ .

222 3. The lower stability of  $A$ - $U$  pairs promotes strand separation, thereby facilitating  
223 the unwinding of the miRNA duplex during RISC loading. Regions rich in  $A$  and  $U$   
224 are thus more likely to undergo strand selection and cleavage events. We assigned  
225  $A$  ( $U$ ) with a larger absolute value than  $G$  ( $C$ ) to reflect this functional relevance.  
226 It aims to highlight sequence regions with higher cleavage potential.

227 It results in our baseline transformation method, namely “Single value mapping” ,  
228 shown in row 1 of Table 4.

229 With the assigned value to each nucleotide defined in single-value mapping, we can  
230 compute a cumulative sum of those values over time. It captures the aggregated signal  
231 by accumulating past events, allowing us to focus on the trend [27, 28]. We named  
232 this method as “Cumulative mapping”, shown in row 4 of Table 4.

### 233 2.2.2 Grouped variable-length channel versus Grouped 234 local-length channel

235 We can transform the input strand into a multivariate time series with two channels  
236 using grouped binary encoding, where nucleotides are grouped into ( $A$ ,  $U$ ) and ( $G$ ,  
237  $C$ ). It releases our third assumption that  $A$  ( $U$ ) has a larger absolute value than  
238  $G$  ( $C$ ). We proposed two variations. The first one allows the output to be variable-  
239 length sequences per channel, depending on group-specific occurrences. The second  
240 one always returns two resulting sequences of fixed length. Two variations extended  
241 from single value mapping are shown in rows 2 and 3, while those extended from  
242 cumulative mapping are shown in rows 5 and 6 in Table 4.

### 243 2.2.3 Global cumulative versus Local Cumulative

244 In cumulative mapping and its variations, we can choose where to start the accumula-  
245 tion. For a given subsequence  $S'$  of the whole sequence  $S$ , accumulation can start  
246 from the beginning of  $S$  even if only  $S'$  is used downstream. Or it can begin just at  
247 the start of the  $S'$ . The first one preserves the global context. It can be useful when  
248 previous nucleotides (those before  $S'$ ) influence later interpretation. The second one  
249 focuses solely on local history in  $S'$ , ignoring global history. It is helpful if the previous  
250 nucleotides do not affect the chemical property of  $S'$ .

251 Consider  $T = 0, -1, \dots, -6$  of the input string  $S$  in “Cumulative mapping” in  
252 Table 4, which accumulates from 0.  $S$  is the suffix with length = 10 of the constructed  
253 complementary strand of  $S(1 : 63)$  in Fig. 1. If we start the accumulation from the  
254 first entry of the constructed complementary strand instead, it will yield a different  
255 result. Suppose the last entry of the time series encoded in the cumulative mapping  
256 of the constructed complementary strand is 2, the time series encoded in the “Global  
257 cumulative mapping” for  $S$  would accumulate from 2 instead of 0. The result is  $T =$   
258  $2, 1, \dots, -4$ . Note that it has the same trend as the original  $T$ . This “Global cumulative”  
259 concept can be applied to every cumulative-based method, as shown in Fig. 3.

### 260 2.2.4 Incorporating base-pair probabilities

261 We can incorporate the base-pair probabilities in the encoding by thinking of it as the  
262 weight or confidence in the value assignment of each nucleotide. It is implemented by

	Encoding	Algorithm	Example
1	Single value mapping [18, 20–23]	$\text{for } i = 1 \text{ to }  S :$ $t_i = \begin{cases} 2 \cdot p_i & \text{if } s_i = A \\ 1 \cdot p_i & \text{if } s_i = G \\ -1 \cdot p_i & \text{if } s_i = C \\ -2 \cdot p_i & \text{if } s_i = U \\ 0 & \text{otherwise} \end{cases}$ $\text{return } T$	$S = C, -, C, U, G, U, U, G, A, U$ $P = 0.843, 0.000, 0.807, 0.807, 0.793,$ $0.914, 0.982, 1.000, 0.999, 0.999$
2	Grouped variable-length channel mapping	$j = 1, k = 1$ $\text{for } i = 1 \text{ to }  S :$ $t_j^1 = \begin{cases} 1 \cdot p_i, & j = j + 1 \text{ if } s_i = A \\ -1 \cdot p_i, & j = j + 1 \text{ if } s_i = U \\ 0, & j = j + 1 \text{ otherwise} \end{cases}$ $t_k^2 = \begin{cases} 1 \cdot p_i, & k = k + 1 \text{ if } s_i = G \\ -1 \cdot p_i, & k = k + 1 \text{ if } s_i = C \\ 0 & \text{otherwise} \end{cases}$ $\text{return } T^1, T^2 // \text{ Only consist of assigned } t_j^1, t_k^2$	Without base-pair probability sequence: $T = -1, 0, -1, -2, 1, -2, -2, 1, 2, -2$ With base-pair probability sequence: $T = -0.843, 0.000, -0.807, -1.614,$ $0.793, -1.829, -1.963,$ $1.000, 1.999, -1.998$
3	Grouped fixed-length channel mapping	$\text{for } i = 1 \text{ to }  S :$ $t_i^1 = \begin{cases} 1 \cdot p_i, & j = j + 1 \text{ if } s_i = A \\ -1 \cdot p_i, & j = j + 1 \text{ if } s_i = U \\ 0 & \text{otherwise} \end{cases}$ $t_i^2 = \begin{cases} 1 \cdot p_i, & k = k + 1 \text{ if } s_i = G \\ -1 \cdot p_i, & k = k + 1 \text{ if } s_i = C \\ 0 & \text{otherwise} \end{cases}$ $\text{return } T^1, T^2$	Without base-pair probability sequence: $T^1 = 0, 0, 0, -1, 0, -1, 0, 1, -1$ $T^2 = -1, 0, -1, 0, 1, 0, 0, 1, 0, 0$ With base-pair probability sequence: $T^1 = 0.000, -0.807, -0.914, -0.982, 0.999, -0.999$ $0.000, -0.914, -0.982,$ $0.000, 0.999, -0.9999$ $T^2 = -0.843, 0.000, -0.807, 0.000,$ $0.793, 0.000, 0.000,$ $1.000, 0.000, 0.000$
4	Cumulative mapping [27, 28]	$t_1 = 0$ $\text{for } i = 1 \text{ to }  S :$ $t_{i+1} = \begin{cases} t_i + 2 \cdot p_i & \text{if } s_i = A \\ t_i + 1 \cdot p_i & \text{if } s_i = G \\ t_i - 1 \cdot p_i & \text{if } s_i = C \\ t_i - 2 \cdot p_i & \text{if } s_i = U \\ t_i & \text{otherwise} \end{cases}$ $\text{return } T //  T  =  S  + 1$	Without base-pair probability sequence: $T = 0, -1, -1, -2, -4, -3, -5, -7, -6, -4, -6$ With base-pair probability sequence: $T = 0.000, -0.843, -0.843, -1.650,$ $-3.265, -2.471, -4.300, -6.263,$ $-5.264, -3.265, -5.263$
5	Cumulative grouped variable-length channel mapping	$t_1^1 = 0, t_1^2 = 0$ $j = 1, k = 1$ $\text{for } i = 1 \text{ to }  S :$ $t_{j+1}^1 = \begin{cases} t_j^1 + 1 \cdot p_i, & j = j + 1 \text{ if } s_i = A \\ t_j^1 - 1 \cdot p_i, & j = j + 1 \text{ if } s_i = U \\ t_j^1, & j = j + 1 \text{ if } s_i = - \end{cases}$ $t_{k+1}^2 = \begin{cases} t_k^2 + 1 \cdot p_i, & k = k + 1 \text{ if } s_i = G \\ t_k^2 - 1 \cdot p_i, & k = k + 1 \text{ if } s_i = C \\ t_k^2 & \text{otherwise} \end{cases}$ $\text{return } T^1, T^2 // \text{ Only consist of assigned } t_j^1, t_k^2$	Without base-pair probability sequence: $T^1 = 0, -1, -2, -3, -2, -3$ $T^2 = 0, -1, -2, -1, 0$ With base-pair probability sequence: $T^1 = 0.000, -0.807, -1.722,$ $-2.703, -1.704, -2.703$ $T^2 = 0.000, -0.843, -1.650,$ $-0.857, 0.143$
6	Cumulative grouped fixed-length channel mapping	$t_1^1 = 0, t_1^2 = 0$ $\text{for } i = 1 \text{ to }  S :$ $t_{i+1}^1 = \begin{cases} t_i^1 + 1 \cdot p_i & \text{if } s_i = A \\ t_i^1 - 1 \cdot p_i & \text{if } s_i = U \\ t_i^1 & \text{otherwise} \end{cases}$ $t_{i+1}^2 = \begin{cases} t_i^2 + 1 \cdot p_i & \text{if } s_i = G \\ t_i^2 - 1 \cdot p_i & \text{if } s_i = C \\ t_i^2 & \text{otherwise} \end{cases}$ $\text{return } T^1, T^2 //  T^1  =  T^2  =  S  + 1$	Without base-pair probability sequence: $T^1 = 0, 0, 0, -1, -2, -3, -3, -2, -3$ $T^2 = 0, -1, -1, -2, -2, -1, -1, 0, 0, 0$ With base-pair probability sequence: $T^1 = 0.000, 0.000, 0.000, 0.000,$ $-0.807, -0.807, -1.722, -2.703,$ $-2.703, -1.704, -2.703$ $T^2 = 0.000, -0.843, -0.843, -1.650,$ $-1.650, -0.857, -0.857, -0.857,$ $0.143, 0.143, 0.143$

**Table 4:** Time series encoding.  $S$  is the first ten nucleotides of the complementary strand of the 3p cleav of “hsa-let-7a-1”, as shown in Table 3.  $P$  is the corresponding base-pair probability sequence.  $p_i = 1$  if we encode  $S$  without base-pair probability sequence.

263 multiplying the base-pair probability  $p_i$  of the nucleotide  $s_i$  with the assigned value  
264 of the kind of nucleotide of  $s_i$  during encoding, as shown in Table 4.

### 265 2.2.5 Transforming the secondary structure into time series

266 We can transform the secondary structure in the dot-bracket notation into a time  
267 series by “Single value mapping”, where “(” maps to 1, “.” maps to 0, and “)” maps  
268 to -1.

## 269 2.3 Time series classification

270 In univariate time series classification, an instance in the dataset consists of a time  
271 series  $x = x_1, x_2, \dots, x_m$  with  $m$  observations and a discrete class label  $y$ , which takes  
272  $c$  possible values [29, 30]. If  $c = 2$ , we refer to binary classification. If  $c > 2$ , we refer  
273 to multi-class classification. In multivariate time series classification, the time series is  
274 not a single sequence but a list of sequences. Each sequence is called a channel. There  
275 are many classifiers defined for time series data, including distance-based, feature-  
276 based, interval-based, shapelet-based, dictionary-based, convolution-based, and deep  
277 learning-based classifiers. Additionally, two or more of the above approaches can be  
278 combined, resulting in hybrid approaches [29–31]. We employed convolution-based  
279 classifiers due to their simplicity and accuracy.

### 280 2.3.1 Convolution-based classifiers

281 Convolution-based classifiers first use randomly parameterized kernels to perform con-  
282 volutions on the original time series  $T$ . Each convolution is performed by sliding a  
283 kernel  $\omega$  across  $T$  and computing a dot product. The output of this process is a time  
284 series, namely an activation map.

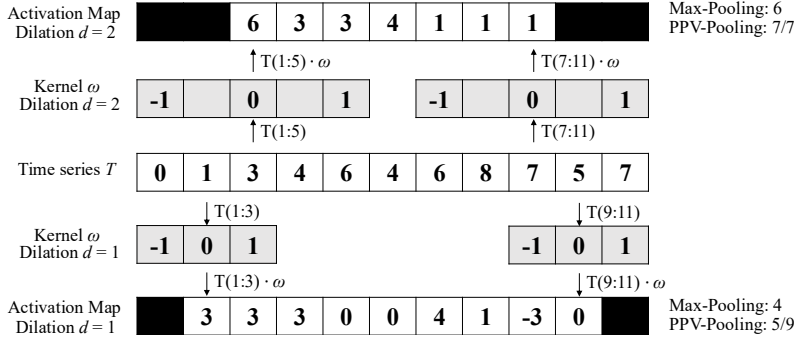


**Fig. 4:** Features generation in the transformation

285 Fig. 4 shows two kernels  $\omega_1$  and  $\omega_2$ , each of which performs convolution with  $T$ .  
286 For example,  $\omega_1$  performs dot product with  $T(1 : 3)$  and result 3 as the first entry of  
287 the activation map. By sliding the kernel one time stamp at a time, an activation map  
288 is produced for each kernel. Then, pooling operations, such as the maximum (MAX)

289 and proportion of positive values (PPV), are applied on the activation map to derive  
290 the summary features.

291 The most popular convolution-based approach is the Random Convolutional Ker-  
292 nel Transform (ROCKET) [32]. It generates a large number of randomly parameterized  
293 kernels, ranging from thousands to tens of thousands. The kernel’s parameters include  
294 length, weights (the entries inside the kernel, which are used for the dot product),  
295 bias (the value added to the result of the convolution operation), and dilation. Addi-  
296 tionally, padding can be applied to the input series at the start and end, ensuring the  
297 activation map has the same length as the input. The summary statistics of the acti-  
298 vation map are obtained through two pooling operations: MAX and PPV. Hence, for  
299  $k$  kernels, the transformed data has  $2k$  features. The default value of  $k$  is 10000.

300 There are two extensions of ROCKET. They are MiniROCKET [33] and Multi-  
301 tIROCKET [34]. MiniROCKET removes unnecessary operations and many of the  
302 random components of ROCKET. It speeds up Rocket by over an order of magnitude  
303 with no significant difference in accuracy, making the classifier almost deterministic.  
304 For example, the kernel length is fixed, and only two weight values are used. Only PPV  
305 is used for the summary statistics. MultiROCKET is extended from MiniROCKET.  
306 The main improvement of it is to extract features from first-order differences and add  
307 three new pooling operations. The three added operations are mean of positive val-  
308 ues (MPV), mean of indices of positive values (MIPV) and longest stretch of positive  
309 values (LSPV).

310 The HYbrid Dictionary-ROCKET Architecture (Hydra) combines dictionary-  
311 based and convolution-based models [35]. Similar to ROCKET-based classifiers, it uses  
312 random kernels to extract features from the input time series. But it groups the ker-  
313 nels into  $g$  groups of  $k$  kernels each. Each time series is passed through all the groups.  
314 For each group of kernels, we slide them across  $T$  and compute the dot product at  
315 each timestamp. Recall that the dot product of two input vectors has the maximum  
316 value when the two vectors align in the same direction and the minimum value when  
317 they are oriented in opposite directions. We record the kernel that best matches the  
318 subsequence of  $T$  at each timestamp in each group. This results in a  $k$ -dimensional  
319 count vector for each of the  $g$  groups. This results in a total of  $g \times k$  features, with  
320 default values of  $g = 64$  and  $k = 8$ . In addition to recording the kernel with the max-  
321 imum response, we can also record the kernel with the minimum response, knowing  
322 that this kernel will be the best match with the “inverted” subsequence of  $T$ . Hydra  
323 is applied to both the original time series and its first-order differences. In conclusion,  
324 Hydra generated approximately 1000 features for each instance in our dataset. [35]  
325 found that it can improve the accuracy by concatenating features from Hydra with  
326 features from MultiRocket. This classifier is called MultiROCKET-Hydra.

327 These five classifiers share the same simple design pattern. It involves the overpro-  
328 duction of features followed by a selection strategy. A large number of features (1000  
329  $\sim 50000$ ) are generated for each instance. The features are then fed into a simple linear  
330 classifier. It determines which features are most useful and returns the final classifica-  
331 tion result. A ridge classifier is used in this study. It is a linear classifier that extends  
332 ridge regression to classification tasks by applying a threshold to the predicted values.  
333 It uses L2 regularization to prevent overfitting. The regularization strength is selected

<sup>334</sup> by internal cross-validation. A Ridge classifier is suggested for small datasets, as in  
<sup>335</sup> our case, while a logistic regression classifier is suggested for large datasets [31].

### <sup>336</sup> 2.4 Evaluation metrics

To evaluate the performance of our time series-based classification (MTSC) model, we adopted five standard classification metrics. They are Accuracy (Acc), Specificity (Sp), Sensitivity (Sn), F1 score (F1), and Matthews Correlation Coefficient (MCC) [36].

$$\begin{aligned} Acc &= \frac{TP + TN}{TP + TN + FP + FN} \\ Sp &= \frac{TN}{TN + FP} \\ Sn &= \frac{TP}{TP + FN} \\ F1 &= \frac{2 \times TP}{2 \times TP + FP + FN} \\ MCC &= \frac{TP \times TN - FP \times FN}{\sqrt{(TP + FP)(TP + FN)(TN + FP)(TN + FN)}} \end{aligned}$$

<sup>337</sup> Where TP, TN, FP, and FN are the number of true positives, true negatives, false  
<sup>338</sup> positives, and false negatives, respectively.

To extend a binary metric to multi-class problems, we can treat the data as a collection of binary problems, one for each class. One class is treated as positive while the other classes are treated as negative. Then, the multi-class metrics can be obtained by averaging binary metric calculations across the set of classes. There are different ways to do the averaging. Here, we adopted a macro-averaging approach. It treats each class equally and calculates the mean of the binary metrics. To use *MCC* in the multiclass case, it can be defined in terms of a confusion matrix *C* for *K* classes, where  $C_{i,j}$  is the number of observations that are actually in class *i* and predicted to be in class *j* [37].

$$MCC_{multi} = \frac{c \times s - \sum_k^K p_k \times t_k}{\sqrt{(s^2 - \sum_k^K p_k^2) \times (s^2 - \sum_k^K t_k^2)}}$$

<sup>339</sup> Where  $t_k = \sum_i^K C_{ik}$  (The number of times class *k* actually occurred),  $p_k = \sum_i^K C_{ki}$   
<sup>340</sup> (The number of times class *k* was predicted),  $c = \sum_k^K C_{kk}$  (The total number of  
<sup>341</sup> samples correctly predicted) and  $s = \sum_i^K \sum_j^K C_{ij}$  (The total number of samples).

## <sup>342</sup> 3 Results

<sup>343</sup> In all experiments, the models were trained and tested using 5-fold cross-validation.  
<sup>344</sup> We retrieved 827 empirically validated sequences of pre-miRNAs. There are 5p arm  
<sup>345</sup> and 3p arm in each sequence. For each arm, we defined a cleavage pattern and a non-  
<sup>346</sup> cleavage pattern. Three datasets, namely “5p arm”, “3p arm”, and “multi-class” were

347 constructed by these patterns. We refer to the cleavage patterns as positive instances  
348 and the non-cleavage patterns as negative instances. The 5p arm dataset comprises  
349 827 positive instances and an equal number of negative instances. The 5p arm and 3p  
350 arm datasets are binary-class datasets. The multi-class dataset comprises all patterns  
351 from both the 5p arm and the 3p arm. There are 827 “5p” instances<sup>10</sup>, 827 “3p”  
352 instances, and 1654 negative instances.

353 For every fold in 5-fold cross-validation, the dataset was divided into a training  
354 set and a test set with sizes of 80% and 20% of the whole dataset, respectively. We  
355 kept the class distribution approximately the same in each fold, as it is in the original  
356 dataset. In each fold derived from the 5p arm and 3p arm datasets, the training set  
357 has a size of 1323, and the test set has a size of 331. In each fold derived from the  
358 multi-class dataset, the training set has a size of 2262, and the test set has a size of  
359 662. We reported the average of the five classification metrics.

360 The ROCKET-based classifiers require all channels in the multivariate time series  
361 to have equal length. We applied padding to the shorter channels using the constant  
362 value 100, which does not appear in the original time series. It ensures the padding  
363 does not introduce ambiguity or interfere with the semantic meaning of the encoded  
364 nucleotide signals.

### 365 3.1 Channel ablation study

366 We utilized three types of data as the input features for each instance. They are  
367 (1) the RNA sequence, which consists of the primary strand and its complementary  
368 strand, (2) the secondary structure information, and (3) the base-pair probability  
369 sequence. To input the data into our time series-based classifiers, we converted them  
370 into multivariate time series. The primary strand and its complementary strand are  
371 each encoded into one or two channels, using the encoding methods in Tables 4. For  
372 example, single value mapping encodes a strand in one channel, while grouped variable-  
373 length channel mapping encodes in two channels. The secondary structure information  
374 is converted into a univariate time series. The base-pair probability sequence is already  
375 in numerical form and does not require further transformation. It can be used either as  
376 a standalone channel or incorporated into the encoding of the complementary strand.  
377 We performed a channel ablation study to determine the most informative combination  
378 of the above channels.

379 We referred to the multivariate time series that consists of the channels from the  
380 RNA sequence only as the baseline setting. We added the other channels to this  
381 baseline. It leads to the following configurations (cfgs):

- 382 1. (cfg 1) Baseline: Time series derived only from the RNA sequence.
- 383 2. (cfg 2) Baseline + Secondary structure: Baseline + time series representation of  
384 the secondary structure.
- 385 3. (cfg 3) Baseline + Base-pair probability (Standalone): Baseline + the base-pair  
386 probability sequence as a standalone channel.
- 387 4. (cfg 4) Baseline + Base-Pair probability (Incorporated): Baseline with the base-pair  
388 probability sequence incorporated into the encoding of the complementary strand.

---

<sup>10</sup>cleavage patterns from the 5p arm

Classifier	5p arm				3p arm				multi-class							
	Acc	Sp	Sn	F1	MCC	Acc	Sp	Sn	F1	MCC	Acc	Sp	Sn	F1	MCC	
Baseline (cfg 1)	ROCKET	0.781	0.743	0.819	0.789	0.563	0.790	0.773	0.807	0.793	0.580	0.717	0.838	0.685	0.700	0.538
	MiniROCKET	0.755	0.728	0.782	0.762	0.512	0.788	0.781	0.794	0.789	0.576	0.685	0.823	0.653	0.662	0.486
	MultiROCKET	0.784	0.767	0.801	0.787	0.568	0.803	0.792	0.814	0.805	0.606	0.691	0.830	0.667	0.672	0.501
	Hydra	0.830	0.800	0.860	0.835	0.663	0.808	0.797	0.820	0.810	0.617	0.731	0.844	0.696	0.712	0.560
	MultiROCKET-Hydra	0.796	0.778	0.815	0.800	0.594	0.807	0.767	0.816	0.808	0.614	0.701	0.836	0.681	0.686	0.520
Baseline + Secondary Structure (cfg 2)	ROCKET	<b>0.847</b>	<b>0.832</b>	0.862	<b>0.849</b>	<b>0.695</b>	<b>0.855</b>	0.842	<b>0.868</b>	<b>0.857</b>	<b>0.711</b>	<b>0.836</b>	<b>0.907</b>	<b>0.828</b>	<b>0.833</b>	<b>0.736</b>
	MiniROCKET	0.825	0.807	0.843	0.827	0.655	0.822	0.802	0.843	0.826	0.646	0.823	0.900	0.812	0.818	0.715
	MultiROCKET	0.812	0.803	0.822	0.814	0.626	0.824	0.809	0.839	0.826	0.649	0.796	0.888	0.791	0.792	0.673
	Hydra	0.845	0.816	<b>0.873</b>	<b>0.849</b>	0.691	0.846	0.817	0.874	0.850	0.694	0.830	0.901	0.814	0.826	0.724
	MultiROCKET-Hydra	0.817	0.809	0.826	0.819	0.635	0.825	0.816	0.834	0.826	0.652	0.803	0.891	0.798	0.800	0.684
Baseline + Base-pair probability (Standalone) (cfg 3)	ROCKET	0.842	0.828	0.855	0.844	0.684	<b>0.855</b>	<b>0.856</b>	0.854	0.855	0.710	0.795	0.885	0.783	0.789	0.670
	MiniROCKET	0.817	0.820	0.814	0.816	0.634	0.836	0.834	0.838	0.836	0.673	0.772	0.872	0.757	0.764	0.632
	MultiROCKET	0.822	0.813	0.832	0.824	0.645	0.825	0.831	0.820	0.824	0.651	0.758	0.866	0.747	0.750	0.612
	Hydra	0.846	0.827	0.865	<b>0.849</b>	0.693	0.851	0.840	0.861	0.852	0.702	0.789	0.879	0.769	0.780	0.658
	MultiROCKET-Hydra	0.822	0.809	0.834	0.824	0.644	0.835	0.840	0.830	0.834	0.670	0.759	0.866	0.746	0.750	0.611
Baseline + Base-pair probability (Incorporated) (cfg 4)	ROCKET	0.799	0.771	0.827	0.805	0.600	0.809	0.786	0.832	0.813	0.610	0.737	0.850	0.712	0.724	0.573
	MiniROCKET	0.776	0.756	0.797	0.781	0.554	0.801	0.808	0.794	0.799	0.603	0.705	0.835	0.675	0.684	0.521
	MultiROCKET	0.814	0.801	0.828	0.817	0.630	0.816	0.812	0.820	0.816	0.634	0.726	0.848	0.706	0.712	0.556
	Hydra	0.822	0.787	0.857	0.828	0.647	0.834	0.828	0.840	0.835	0.669	0.759	0.862	0.734	0.746	0.608
	MultiROCKET-Hydra	0.814	0.802	0.820	0.817	0.629	0.820	0.825	0.816	0.819	0.642	0.736	0.853	0.717	0.723	0.874

Table 5: Channel ablation study.

We used single value mapping as the encoding method. Table 5 shows the result. From the table, we can see that the addition of secondary structure, base-pair probability as a standalone channel, and base-pair probability incorporated in the encoding of the complementary strand can improve the performance. We plotted the critical difference (CD) diagram to visualize Table 5 to make the performances of different combinations more obvious. In CD diagrams, lower-ranked methods (toward the right) are better. A horizontal bar connecting combinations indicates no statistically significant difference. From Figure 5, we can see that including time series derived from

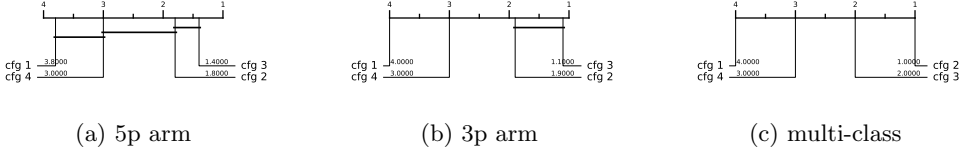


Fig. 5: CD diagrams of channel ablation study.

secondary structure information and base-pair probability as a separate channel can significantly improve the performance of the classifiers. Incorporating the base-pair probability sequence in the time series encoding of the complementary strand can also improve the classifier, but to a minor degree compared to serving as a standalone channel. In our downstream analysis, we adopted the combination of RNA sequence time series, secondary structure time series, and base-pair probability time series as our multivariate time series input, with 4 to 6 channels, depending on the encoding used.

### 3.2 Predictive performance

The experiment was conducted on three datasets: the 5p arm, the 3p arm, and the multi-class datasets. Recall that we have nine encoding methods and five ROCKET-based classifiers. It results in 45 combinations of encoding methods and classifiers.

Classifier	5p arm					3p arm					multi-class						
	Acc	Sp	Sn	F1	MCC	Acc	Sp	Sn	F1	MCC	Acc	Sp	Sn	F1	MCC		
Single value mapping (enc 1)	ROCKET	0.849	0.842	0.857	0.851	0.699	0.863	0.854	0.873	0.865	0.727	0.853	0.917	0.847	0.851	0.764	
	MiniROCKET	0.823	0.809	0.837	0.825	0.647	0.823	0.828	0.817	0.822	0.647	0.835	0.906	0.828	0.833	0.735	
	MultiROCKET	0.821	0.802	0.848	0.824	0.643	0.839	0.826	0.852	0.841	0.679	0.811	0.894	0.806	0.809	0.697	
	Hydra	0.843	0.820	0.867	0.847	0.688	0.838	0.819	0.857	0.841	0.677	0.831	0.901	0.815	0.827	0.727	
Grouped variable-length channel mapping (enc 2)	ROCKET	0.835	0.826	0.844	0.836	0.670	0.855	0.849	0.861	0.856	0.710	0.846	0.913	0.839	0.844	0.752	
	MiniROCKET	0.843	0.833	0.853	0.844	0.686	0.831	0.821	0.842	0.833	0.663	0.837	0.907	0.828	0.834	0.737	
	MultiROCKET	0.819	0.809	0.829	0.820	0.638	0.817	0.814	0.820	0.818	0.634	0.890	0.894	0.806	0.803	0.695	
	Hydra	0.825	0.780	0.869	0.832	0.653	0.811	0.768	0.854	0.819	0.626	0.818	0.892	0.765	0.812	0.705	
Grouped fixed-length channel mapping (enc 3)	ROCKET	0.851	0.843	0.859	0.859	0.702	0.863	0.850	0.875	0.864	0.726	0.849	0.915	0.843	0.847	0.752	
	MiniROCKET	0.844	0.839	0.853	0.845	0.689	0.840	0.826	0.855	0.843	0.682	0.851	0.915	0.844	0.848	0.760	
	MultiROCKET	0.831	0.815	0.848	0.834	0.663	0.824	0.813	0.836	0.826	0.649	0.811	0.896	0.808	0.808	0.698	
	Hydra	0.848	0.816	0.880	0.853	0.699	0.862	0.839	0.884	0.864	0.724	0.843	0.908	0.837	0.839	0.746	
Cumulative mapping (enc 4)	ROCKET	0.850	0.834	0.866	0.852	0.701	0.863	0.855	0.871	0.864	0.726	0.852	0.915	0.842	0.850	0.762	
	MiniROCKET	0.840	0.821	0.860	0.843	0.682	0.840	0.837	0.844	0.841	0.682	0.843	0.911	0.835	0.840	0.747	
	MultiROCKET	0.822	0.809	0.834	0.824	0.644	0.832	0.830	0.834	0.832	0.665	0.820	0.898	0.810	0.816	0.709	
	Hydra	0.848	0.819	0.874	0.853	0.699	0.853	0.856	0.869	0.855	0.705	0.845	0.910	0.830	0.841	0.749	
Cumulative grouped variable-length channel mapping (enc 5)	ROCKET	0.843	0.821	0.866	0.847	0.688	0.840	0.871	0.871	0.857	0.712	0.855	0.916	0.843	0.851	0.766	
	MiniROCKET	0.845	0.826	0.865	0.848	0.691	0.836	0.833	0.838	0.836	0.672	0.840	0.909	0.833	0.838	0.742	
	MultiROCKET	0.826	0.814	0.836	0.828	0.658	0.815	0.820	0.810	0.814	0.631	0.826	0.902	0.820	0.824	0.721	
	Hydra	0.850	0.819	0.880	0.854	0.701	0.834	0.807	0.861	0.836	0.669	0.833	0.903	0.818	0.829	0.731	
Cumulative grouped fixed-length channel mapping (enc 6)	ROCKET	0.856	0.836	0.876	0.858	0.712	0.870	<b>0.870</b>	<b>0.861</b>	<b>0.879</b>	<b>0.871</b>	<b>0.741</b>	0.863	<b>0.921</b>	<b>0.852</b>	<b>0.860</b>	<b>0.780</b>
	MiniROCKET	0.856	0.837	0.874	0.858	0.712	0.842	0.839	0.845	0.843	0.685	0.845	0.912	0.837	0.843	0.751	
	MultiROCKET	0.820	0.802	0.839	0.824	0.642	0.798	0.798	0.798	0.798	0.597	0.809	0.894	0.806	0.807	0.694	
	Hydra	0.850	0.814	0.885	0.855	0.701	0.855	0.840	0.869	0.857	0.711	0.847	0.910	0.831	0.843	0.752	
Global Cumulative mapping (enc 7)	ROCKET	0.850	0.834	0.866	0.852	0.701	0.863	0.855	0.871	0.864	0.726	0.852	0.915	0.842	0.850	0.762	
	MiniROCKET	0.847	0.832	0.862	0.849	0.695	0.848	0.839	0.857	0.850	0.697	0.845	0.911	0.836	0.843	0.750	
	MultiROCKET	0.827	0.819	0.834	0.828	0.653	0.847	0.842	0.853	0.848	0.695	0.825	0.901	0.817	0.822	0.718	
	Hydra	0.851	0.821	0.880	0.855	0.703	0.861	0.848	0.874	0.863	0.722	0.847	0.911	0.834	0.844	0.753	
Global Cumulative grouped variable-length channel mapping (enc 8)	ROCKET	0.829	0.823	0.834	0.830	0.658	0.843	0.838	0.849	0.844	0.688	0.832	0.905	0.823	0.829	0.730	
	MiniROCKET	0.840	0.814	0.867	0.844	0.688	0.853	0.838	0.867	0.854	0.706	0.856	0.917	0.845	0.853	0.768	
	MultiROCKET	0.848	0.834	0.862	0.850	0.697	0.841	0.824	0.859	0.844	0.683	0.844	0.911	0.856	0.842	0.748	
	Hydra	0.834	0.828	0.839	0.834	0.668	0.831	0.821	0.842	0.833	0.663	0.828	0.904	0.826	0.826	0.724	
Global Cumulative grouped fixed-length channel mapping (enc 9)	ROCKET	0.856	0.836	0.876	0.858	0.712	<b>0.870</b>	<b>0.861</b>	<b>0.879</b>	<b>0.871</b>	<b>0.741</b>	0.863	<b>0.921</b>	<b>0.852</b>	<b>0.860</b>	<b>0.780</b>	
	MiniROCKET	<b>0.857</b>	<b>0.845</b>	<b>0.870</b>	<b>0.850</b>	<b>0.715</b>	0.840	0.821	0.859	0.843	0.681	0.844	0.911	0.837	0.842	0.749	
	MultiROCKET	0.829	0.825	0.833	0.830	0.658	0.820	0.816	0.823	0.820	0.640	0.819	0.900	0.816	0.817	0.710	
	Hydra	0.856	0.817	0.894	0.861	0.713	0.859	0.838	0.880	0.862	0.719	0.846	0.911	0.832	0.843	0.752	
MultiROCKET-Hydra	ROCKET	0.829	0.824	0.834	0.830	0.658	0.822	0.825	0.819	0.821	0.644	0.827	0.904	0.823	0.824	0.722	

**Table 6:** Performance on the 45 combinations between encoding methods and the ROCKET-based classifiers.

The result is shown in Table 6. The best combination of encoding method and classifier is shown in Table 7. For the 5p arm dataset, the best combination is “Global Cumulative grouped fixed-length channel mapping + ROCKET”. For all five classification metrics, it outperforms the state-of-the-art (SOTA) method, DiCleave. For the 3p arm dataset, the best combination is “Global Cumulative grouped fixed-length channel mapping + ROCKET”. Out of the five classification metrics, it outperforms DiCleave, except in specificity. For the multi-class dataset, the best combination is “Global Cumulative grouped fixed-length channel mapping + ROCKET”. For all five classification metrics, it outperforms DiCleave. Note that for the 3p arm and the multi-class datasets, the combination of “Cumulative grouped fixed-length channel mapping + ROCKET” also attains the best result.

To summarize Table 6, we plot the CD diagrams for finding the best classifier, as shown in Figure 6, and the best encoding method, as shown in Figure 7.

### 3.3 Running time analysis

To compare the computational efficiency of MTSCCleav and DiCleave, we conducted a comparative analysis of their running times. For DiCleave, we employed the code from

Dataset	Methods	Acc	Sp	Sn	F1	MCC	Time (s)
5p arm	enc 9 + MiniROCKET	<b>0.857</b>	<b>0.845</b>	<b>0.870</b>	<b>0.859</b>	<b>0.715</b>	<b>0.787</b>
	DiCleave	0.818	0.790	0.846	0.822	0.653	21.249
3p arm	enc 9 + ROCKET	<b>0.870</b>	0.861	<b>0.879</b>	<b>0.871</b>	<b>0.741</b>	4.311
	enc 7 + MiniROCKET	0.848	0.839	0.857	0.850	0.697	<b>0.989</b>
	DiCleave	0.854	<b>0.891</b>	0.817	0.847	0.715	15.919
multi-class	enc 9 + ROCKET	<b>0.863</b>	<b>0.921</b>	<b>0.852</b>	<b>0.860</b>	<b>0.780</b>	12.208
	enc 3 + MiniROCKET	0.851	0.915	0.844	0.849	0.760	<b>4.550</b>
	DiCleave	0.820	0.895	0.804	0.815	0.710	131.151

**Table 7:** Comparative analysis between MTSCleav with the best combination of the encoding method and classifier, with the SOTA, DiCleave, on the three datasets. The best results of using MiniROCKET have also been shown to compare the computational efficiency.

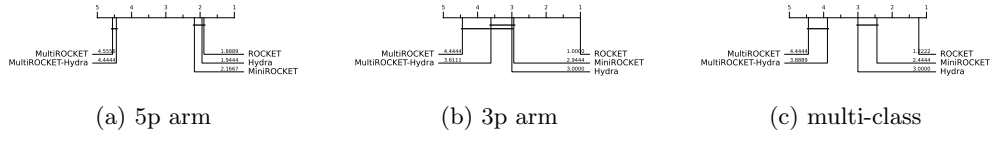


**Fig. 6:** CD diagrams to compare different classifiers.

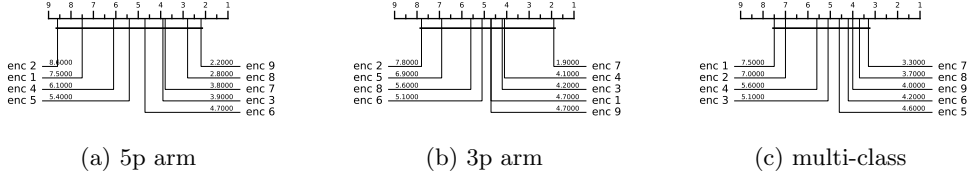


**Fig. 7:** CD diagrams to compare different encoding methods.

its supporting website<sup>11</sup>, without any modifications. All experiments were conducted on the same machine (a personal laptop equipped with an Apple M1 Pro chip and 16 GB of memory) and using the same splits of the training and test datasets under 5-fold cross-validation to ensure fairness. The reported running times are the averages of the five runs. The timing results were measured from the training phase to the return of the five classification metrics. The result is shown in Table 7. MiniROCKET is the most computationally efficient of the five rocket-based classifiers. We also included its best result, along with the corresponding encoding method, even though this combination may not be the best overall.

11

<https://github.com/MGuard0303/DiCleave> (Accessed on: 2025-07-13).

433 MTSCCleav demonstrated a significant advantage in computational efficiency,  
434 achieving an average 27.0X, 3.7X, and 10.7X speedup over DiCleave, for the 5p arm,  
435 3p arm, and multi-class datasets, respectively. If we consider using the MiniROCKET  
436 in the case of 3p arm and multi-class datasets, it achieves 16.1X and 28.8X speedup.  
437 To note, in the case of the 3p arm dataset, the performance of MiniROCKET is only  
438 slightly lower than DiCleave. In the case of the multi-class dataset, even the perfor-  
439 mance of MiniROCKET is better than DiCleave. DiCleave is a deep learning-based  
440 method that requires substantial time for model inference, while MTSCCleav lever-  
441 ages efficient ROCKET-based classifiers. This significant reduction in runtime makes  
442 MTSCCleav more suitable for large-scale data and real-time applications.

### 443 3.4 Subsequence importance

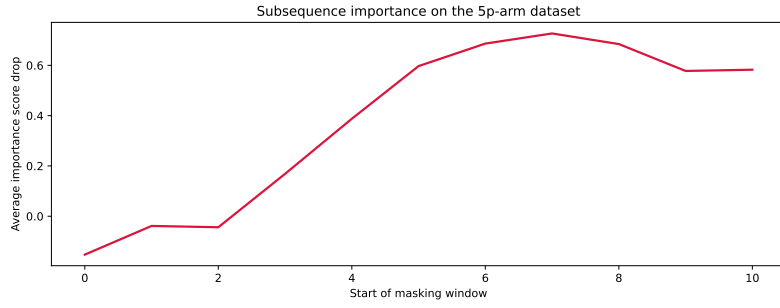
444 To evaluate the sensitivity of MTSCCleav to subsequences of the input, we conducted a  
445 perturbation experiment to evaluate the importance of subsequences based on masking  
446 windows. The goal of this experiment is to identify which subsequences of the entire  
447 time series are critical for classification. We examine how various modifications to the  
448 original input impact model performance. It suggests which features are essential for  
449 classification.

450 The model was trained on the original training dataset. For each instance in the  
451 test dataset, we measure its original score and the masked score. We slid a masking  
452 window  $w$  with a fixed length over the input time series  $T$ .  $|w|$  was set to 4. For each  
453 window position  $i \in \{1, 2, \dots, |T|-|w|+1\}$ , we masked all entries across all the channels  
454 of  $T$  within the window. Hence, we removed or hid that portion of information from  
455 the model during inference. The changes in classification performance in terms of  
456 accuracy relative to the unmasked original score of each  $i$  are recorded. Intuitively, if  
457 the information of a subsequence is critical for the classification, the masking of this  
458 subsequence would lead to a great drop in classification performance. We aggregated  
459 the importance score across the test dataset. The result is shown in Figure 8. For the  
460 encoding methods, we cannot use the methods derived from the cumulative mapping  
461 because the accumulation would leak information from the masked region. We adopted  
462 “Grouped fixed-length channel mapping” as the encoding method and ROCKET as  
463 the classifier. “Grouped fixed-length channel mapping” is the best encoding, other  
464 than the methods derived from the cumulative mapping, in all datasets, as shown in  
465 Figure 7. ROCKET is the best classifier, as shown in Figure 6..

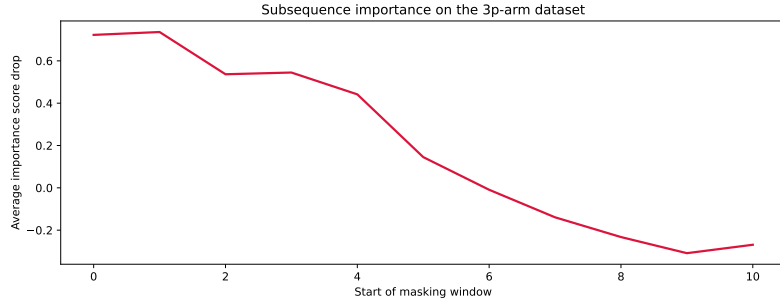
466 In the 5p arm dataset, we found that masking subsequences at the tailing part  
467 caused a significant drop in the importance score, as shown in Figure 8 (a). In the  
468 3p arm dataset, we found that masking subsequences at the leading part caused a  
469 significant drop in the importance score, as shown in Figure 8 (b).

## 470 4 Discussion

471 The channel ablation study reveals that the involvement of the time series derived  
472 from the secondary structure can improve accuracy. It suggests the importance of  
473 RNA folding in dicer processing. Additionally, we found that the base-pair probabili-  
474 ty sequence of the secondary structure can also enhance accuracy. To the best of our



(a) 5p arm



(b) 3p arm

**Fig. 8:** Results of the perturbation experiment.

knowledge, it is a novel application of the base-pair probability sequence. Experiments show that using the probability sequence as an additional channel can enhance accuracy more than incorporating it in the encoding. It is likely because keeping it as an additional channel can preserve more information, of both the probability sequence itself and the complementary strand.

Out of the three datasets, the best classifier is ROCKET. The ranking of the five classifiers by performance, starting from the best, is as follows: ROCKET, Hydra, MiniROCKET, MultiROCKET-Hydra, and MultiROCKET. It indicates that the features created from the pooling operations that are only in MultiROCKET but not in MiniROCKET, confuse the final classifier. They are mean of positive values (MPV), mean of indices of positive values (MIPV) and longest stretch of positive values (LSPV) [34]. In contrast, the pooling operator that is only present in ROCKET but not in MiniROCKET, enhances the classification performance. It is maximum (MAX).

For the encoding methods, we have the following observations. Fixed-length grouped channel mappings outperform variable-length counterparts with one exception in the multi-class dataset, likely because fixed-length schemes better preserve the original positional information of nucleotides within the sequence. Global cumulative methods consistently yield better performance than local cumulative methods.

493 It suggests that the upstream information of the cleavage pattern plays a critical role  
494 in identifying cleavage sites. Cumulative-based encodings perform better than single-  
495 value mappings, with one exception in the 3p dataset, suggesting that the accumulated  
496 nucleotide signal is more informative for cleavage site prediction than the local or iso-  
497 lated presence of nucleotides. In the 5p arm dataset, encoding RNA sequence in two  
498 channels appears to worsen the result. This suggests that the 5p arm dataset and the  
499 3p arm dataset need different nucleotide grouping methods for the encoding.

500 One limitation of DiCleave is overfitting during training because of the relatively  
501 small size of the dataset [11]. DiCleave is a deep learning-based method. Deep learning  
502 models typically require a large amount of training data to generalize effectively. They  
503 are data-hungry. In contrast, MTSCCleav leverages ROCKET-based methods for the  
504 classification. They rely on random convolutional feature extraction followed by a sim-  
505 ple linear classifier. The Ridge classifier used in this study is less data-hungry compared  
506 to deep learning methods due to its use of L2 regularization and the simplicity of its  
507 linear model nature. It allows ROCKET-based classifiers, and hence MTSCCleav, to  
508 maintain strong predictive performance even in settings with a relatively small dataset  
509 size.

510 The subsequence importance reveals some connections between RNA secondary  
511 structure and human dicer cleavage site prediction. The perturbation experiment  
512 shows that the leading part of 5p arm and the tailing part of 3p arm are important  
513 for the classification. These parts are close to the center of the RNA secondary struc-  
514 ture of pre-miRNA. It indicates that the center region is more crucial for human dicer  
515 cleavage site prediction. It agrees with the previous study [10].

## 516 5 Conclusions

517 We proposed an accurate, fast, and simple multivariate time series classification  
518 (MTSC)-based method, termed MTSCCleav, for predicting human dicer cleavage sites.  
519 Base-pair probability sequences of the secondary structures have also been leveraged  
520 in the classification. MTSCCleav consists of three parts: time series encoding, time  
521 series transformation, and classification. ROCKET-based methods were used for time  
522 series transformation. Ridge Classifier was used for classification. For the computa-  
523 tional experiments, we evaluated nine time series encoding methods in conjunction  
524 with five time series transformation methods. MTSCCleav outperformed the SOTA  
525 method in all five evaluation metrics for the 5p-arm and multi-class datasets, and four  
526 of the metrics for the 3p-arm dataset. In terms of computational efficiency, MTSC-  
527 Cleav with the optimal setting achieved an average 3.7X to 27.0X speedup over the  
528 SOTA method on the three datasets. With the use of a less accurate but faster time  
529 series transformation method, MTSCCleav achieved an average speedup of 16.1X to  
530 28.8X, respectively. We analyzed the subsequence importance of the input multivari-  
531 ate time series. The results show that subsequences near the center of the pre-miRNA  
532 sequences are more important. This aligns with the findings from previous work. This  
533 study demonstrates that time series analysis provides a powerful alternative to conven-  
534 tional modeling in the context of RNA processing. This framework may be extended to

535 other RNA-processing tasks. Notably, the encoding of RNA sequence into time series  
536 enables us to utilize any well-established tools from the time series community.

## 537 References

- 538 [1] Urry, L.A., Cain, M.L., Wasserman, S.A., Minorsky, P.V., Orr, R.B., Campbell,  
539 N.A.: *Campbell Biology*, Twelfth edition edn., New York, NY (2020)
- 540 [2] Alberts, B.: *Molecular Biology of the Cell*, Seventh edition edn., New York (2022)
- 541 [3] Cohen, W.W.: *A Computer Scientist's Guide to Cell Biology: A Travelogue from*  
542 *a Stranger in a Strange Land*, New York, NY (2007)
- 543 [4] Lee, Y., Jeon, K., Lee, J.-T., Kim, S., Kim, V.N.: Microrna maturation: Stepwise  
544 processing and subcellular localization. *The EMBO Journal* **21**(17), 4663–4670  
545 (2002)
- 546 [5] Gu, S., Jin, L., Zhang, Y., Huang, Y., Zhang, F., Valdmanis, P.N., Kay, M.A.:  
547 The loop position of shrnas and pre-mirnas is critical for the accuracy of dicer  
548 processing *in vivo*. *Cell* **151**(4), 900–911 (2012)
- 549 [6] Feng, Y., Zhang, X., Graves, P., Zeng, Y.: A comprehensive analysis of precursor  
550 microrna cleavage by human dicer. *RNA* **18**(11), 2083–2092 (2012)
- 551 [7] MacRae, I.J., Zhou, K., Doudna, J.A.: Structural determinants of rna recognition  
552 and cleavage by dicer. *Nature Structural & Molecular Biology* **14**(10), 934–940  
553 (2007)
- 554 [8] Ahmed, F., Kaundal, R., Raghava, G.P.: Phdcleav: A svm based method for  
555 predicting human dicer cleavage sites using sequence and secondary structure of  
556 mirna precursors. *BMC Bioinformatics* **14**(14), 9 (2013)
- 557 [9] Bao, Y., Hayashida, M., Akutsu, T.: Lbsizecleav: Improved support vector  
558 machine (svm)-based prediction of dicer cleavage sites using loop/bulge length.  
559 *BMC Bioinformatics* **17**(1), 487 (2016)
- 560 [10] Liu, P., Song, J., Lin, C.-Y., Akutsu, T.: Recgbm: A gradient boosting-based  
561 method for predicting human dicer cleavage sites. *BMC Bioinformatics* **22**(1), 63  
562 (2021)
- 563 [11] Mu, L., Song, J., Akutsu, T., Mori, T.: Dicleave: A deep learning model for  
564 predicting human dicer cleavage sites. *BMC Bioinformatics* **25**(1), 13 (2024)
- 565 [12] Mu, L., Akutsu, T.: DiCleavePlus: A Transformer-Based Model to Detect Dicer  
566 Cleavage Sites within Cleavage Patterns. Submitted, under review (2025). <https://github.com/MGuard0303/DiCleavePlus>

- 568 [13] Griffiths-Jones, S., Saini, H.K., van Dongen, S.: mirbase: Tools for microRNA  
569 genomics. *Nucleic Acids Research* **36**(suppl\_1), 154–158 (2008)
- 570 [14] Xu, T., Su, N., Liu, L., Zhang, J., Wang, H., Zhang, W., Gui, J., Yu, K., Li, J., Le,  
571 T.D.: mirbaseconverter: An r/bioconductor package for converting and retrieving  
572 mirna name, accession, sequence and family information in different versions of  
573 mirbase. *BMC Bioinformatics* **19**(19), 514 (2018)
- 574 [15] Zvelebil, M.J., Baum, J.O., Zvelebil, M.: Understanding Bioinformatics, New York  
575 (2008)
- 576 [16] Lorenz, R., Bernhart, S.H., Höner zu Siederdissen, C., Tafer, H., Flamm, C.,  
577 Stadler, P.F., Hofacker, I.L.: Viennarna package 2.0. *Algorithms for Molecular  
578 Biology* **6**(1), 26 (2011)
- 579 [17] Aggarwal, C.C.: Data Mining: The Textbook, Cham (2015)
- 580 [18] Mendizabal-Ruiz, G., Román-Godínez, I., Torres-Ramos, S., Salido-Ruiz, R.A.,  
581 Morales, J.A.: On dna numerical representations for genomic similarity compu-  
582 tation. *PLOS ONE* **12**(3), 0173288 (2017)
- 583 [19] Anastassiou, D.: Genomic signal processing. *IEEE Signal Processing Magazine*  
584 **18**(4), 8–20 (2001)
- 585 [20] Rakthanmanon, T., Campana, B., Mueen, A., Batista, G., Westover, B., Zhu, Q.,  
586 Zakaria, J., Keogh, E.: Searching and mining trillions of time series subsequences  
587 under dynamic time warping. In: *Proceedings of the 18th ACM SIGKDD Interna-*  
588 *tional Conference on Knowledge Discovery and Data Mining. KDD '12*, pp.  
589 262–270, New York, NY, USA (2012)
- 590 [21] Cristea, P.D.: Conversion of nucleotides sequences into genomic signals. *Journal  
591 of Cellular and Molecular Medicine* **6**(2), 279–303 (2002)
- 592 [22] Chakravarthy, N., Spanias, A., Iasemidis, L.D., Tsakalis, K.: Autoregressive mod-  
593 eling and feature analysis of dna sequences. *EURASIP Journal on Advances in  
594 Signal Processing* **2004**(1), 1–16 (2004)
- 595 [23] Zhao, J., Yang, X.W., Li, J.P., Tang, Y.Y.: Dna sequences classification based on  
596 wavelet packet analysis. In: *Wavelet Analysis and Its Applications*, pp. 424–429  
597 (2001)
- 598 [24] Holden, T., Subramaniam, R., Sullivan, R., Cheung, E., Schneider, C., Jr, G.T.,  
599 Flamholz, A., Lieberman, D.H., Cheung, T.D.: Atcg nucleotide fluctuation of  
600 deinococcus radiodurans radiation genes. In: *Instruments, Methods, and Missions  
601 for Astrobiology X*, vol. 6694, pp. 402–411 (2007)
- 602 [25] Nair, A.S., Sreenadhan, S.P.: A coding measure scheme employing electron-ion

- 603 interaction pseudopotential (eiip). *Bioinformation* **1**(6), 197–202 (2006)
- 604 [26] Akhtar, M., Epps, J., Ambikairajah, E.: On dna numerical representations  
605 for period-3 based exon prediction. In: 2007 IEEE International Workshop on  
606 Genomic Signal Processing and Statistics, pp. 1–4 (2007)
- 607 [27] Zhang, R., Zhang, C.-T.: Z curves, an intutive tool for visualizing and analyzing  
608 the dna sequences. *Journal of Biomolecular Structure and Dynamics* **11**(4), 767–  
609 782 (1994)
- 610 [28] Berger, J.A., Mitra, S.K., Carli, M., Neri, A.: Visualization and analysis of dna  
611 sequences using dna walks. *Journal of the Franklin Institute* **341**(1), 37–53 (2004)
- 612 [29] Bagnall, A., Lines, J., Bostrom, A., Large, J., Keogh, E.: The great time series  
613 classification bake off: A review and experimental evaluation of recent algorithmic  
614 advances. *Data Mining and Knowledge Discovery* **31**(3), 606–660 (2017)
- 615 [30] Ruiz, A.P., Flynn, M., Large, J., Middlehurst, M., Bagnall, A.: The great multi-  
616 variate time series classification bake off: A review and experimental evaluation  
617 of recent algorithmic advances. *Data Mining and Knowledge Discovery* **35**(2),  
618 401–449 (2021)
- 619 [31] Middlehurst, M., Schäfer, P., Bagnall, A.: Bake off redux: A review and experi-  
620 mental evaluation of recent time series classification algorithms. *Data Mining and  
621 Knowledge Discovery* **38**(4), 1958–2031 (2024)
- 622 [32] Dempster, A., Petitjean, F., Webb, G.I.: Rocket: Exceptionally fast and accurate  
623 time series classification using random convolutional kernels. *Data Mining and  
624 Knowledge Discovery* **34**(5), 1454–1495 (2020)
- 625 [33] Dempster, A., Schmidt, D.F., Webb, G.I.: Minirocket: A very fast (almost) deter-  
626 ministic transform for time series classification. In: Proceedings of the 27th ACM  
627 SIGKDD Conference on Knowledge Discovery & Data Mining. KDD '21, pp.  
628 248–257, New York, NY, USA (2021)
- 629 [34] Tan, C.W., Dempster, A., Bergmeir, C., Webb, G.I.: Multirocket: Multiple pool-  
630 ing operators and transformations for fast and effective time series classification.  
631 *Data Mining and Knowledge Discovery* **36**(5), 1623–1646 (2022)
- 632 [35] Dempster, A., Schmidt, D.F., Webb, G.I.: Hydra: Competing convolutional ker-  
633 nels for fast and accurate time series classification. *Data Mining and Knowledge  
634 Discovery* **37**(5), 1779–1805 (2023)
- 635 [36] Matthews, B.W.: Comparison of the predicted and observed secondary structure  
636 of t4 phage lysozyme. *Biochimica et Biophysica Acta (BBA) - Protein Structure*  
637 **405**(2), 442–451 (1975)

- <sup>638</sup> [37] Gorodkin, J.: Comparing two k-category assignments by a k-category correlation  
<sup>639</sup> coefficient. Computational Biology and Chemistry **28**(5), 367–374 (2004)